# Range and Doppler walk in DVB-T based Passive Bistatic Radar

Jonas Myhre Christiansen
Norwegian Defence Research Establishment
Kjeller, Norway
Email: Jonas-Myhre.Christiansen@ffi.no

Karl Erik Olsen
Norwegian Defence Research Establishment
Kjeller, Norway
Email: Karl-Erik.Olsen@ffi.no

*Abstract*—This paper analyzes the effects of range and Doppler walk for a Digital Video Broadcast - Terrestrial based Passive Bistatic Radar of both simulated and experimental data. Range and Doppler walk cause energy dispersal in the correlation, thus the coherent integration time is limited by the bistatic velocity and acceleration. A method using the readily available Doppler information to compensate for the range displacement during integration due to non-zero bistatic velocity of target is described. By compensating and non-coherently adding several coherently processed intervals, the target signal to noise ratio is increased.

## I. Introduction

Passive Coherent Location (PCL), Passive Covert Radar (PCR), or Passive Bistatic Radar (PBR), in this paper referred to as PBR, [1, pp. 248–249], has received much interest in the academic as well as military communities. Since the end of World War II the interest for bistatic radars has been going in cycles with a periodicity of 15 to 20 years [2], and the most successful bistatic radar application since then has been the semiactive homing missiles. However, the interest for bistatic or multistatic radars is at the moment at a definite peak, mainly due to the rapidly emerging PBR technology. According to [3, pp 78], "passive bistatic radars (PBRs) are a subset of bistatic radars that exploit non radar transmitters of opportunity as their source of illumination". The bistatic radar theory is readily available in [4], and on PBR especially in [3].

The claimed military benefits from operating a passive sensor in the VHF/UHF[1] radar frequency range are among the main drivers behind the interest. This is backed by the two competing FM radio based PBR systems under testing from Lockheed Martin, Silent Sentry 3 [5], and from Thales, Home Alerter 100 [6], participating in trials arranged with potential customers. Through official channels high level results and performances are reported. In parallel, the unclassified/open research is ongoing at universities and research facilities around the world. The majority of this research has been focused on the signal and waveform availability [7], [8], [9], [10], [11], [12], [13],

[14] and the detection performance of PBR systems [15], [16], [17], [6], [18], [19], [20], [21], [22], [1], [23], and finally multifrequency fusing of data from similar as well as different PBR systems relying on FM radio, DAB and DVB-T transmitters of opportunity in order to improve target detection [6], [18], [19], [13], [20], [21]. No traces of work considering range and Doppler walk in PBR systems has been found, although [1, pp. 126] and [22, pp. 255] formulate the problem.

It has been shown that in order to achieve ranges of interest for air surveillance applications, the PBR system has to rely on one of the three broadcasters of opportunity: FM radio, DAB or DVB-T, as shown in [1], [7], [9], [10]. Of these, the DVB-T systems stands out due to its relatively high bandwidth in each channel, $6 - 8MHz$ compared to FM radio $100 - 200kHz$, and DAB $1.5 - 2MHz$. However, using a DVB-T[2] broadcaster as a transmitter of opportunity in a PBR system, we may be facing the problems of both range and Doppler walk. The bandwidth of the Norwegian DVB-T OFDM signal is $B = 7.61MHz$, resulting in a bistatic range resolution of $R_B = c/B \approx 39.4m$, where $c$ is the speed of propagation. A target travelling in $200m/s$ migrates through 5 range cells during one second of coherent integration time, and one second of coherent integration time $\tau = 1sec$ results in Doppler resolution of $\Delta f = 1/\tau = 1Hz$, in which a target will not stay for longer periods. This results in a spreading in both Doppler and range. In order to achieve sufficient $S/N$-ratio for detection ranges comparable to FM radio systems, coherent integration times $\tau$ up to one second should be applied [1], [22]. Very few details on this are available in the open literature, however Thales reported integration times up to 0.1s for their DVB-T demonstrator [6].

For SAR/ISAR applications, the problems of range and Doppler walk are well established [24, pp. 370–380], where the target's translational motion is causing both range walk (moving through range cells during integration), and range offset (the Doppler shift results in a ranging error due to the chirped waveform and the demodulation of this). The change of target velocity with respect to the

---

[1]VHF - Very High Frequency (30-300MHz), UHF - Ultra High Frequency (300-1000MHz) in the IEEE Radar Designation

[2]The range and Doppler walk will also be present in the DAB PBR system, although not to such extent as in the DVB-T based PBR system.

radar during integration, Doppler walk, will cause the final image to be smeared, and target velocity models and/or motion correction algorithms are applied to counter those problems [24], where the effects of range walk (and range offset) for chirp-pulse and stepped frequency waveforms are treated, and performance figures for range walk degradation as a function of integration time is calculated.

This work is focusing on applying the OFDM waveform in the matced filter processing, and are thus not suffering from the range offset problem as described in [24]. Further, we are only interested in compensating for the translational motion with respect to the radar, and not the rotational motion, additionally simplifying the situation. We will in this work apply the digital counterpart to the work in [25], where an analog implementation of multiple range delay lines for each of the Doppler filters are applied in order to align the time varying responses from the moving target.

Our constraints arise from the fact that we are focusing on improving the detection probability of targets without at the same time massively increasing the computational load in the receiver. This can be readily achieved by applying the basic ideas from [24, pp. 370–380], and [25], in which the matched filter processing can be performed extremely efficiently by using FFT/IFFT methods, and with only simple manipulation of the collected data before the processing we can align the time varying responses from the moving target, as well as the time varying Doppler response. The method will work on all targets, at all ranges, at all Doppler velocities without any need for detection of the target during processing, nor any other a priori information on the target. The method is applied on simulated as well as real life data from an experimental PBR system, resulting in a generic model for performance estimates, verified by real life measurments.

## II. DVB-T SYSTEM

The transmission is based on OFDM modulation, and the video and audio data streams are encoded using MPEG and then interleaved, leading to a randomization of the data bit stream. According to [26], the transmission signal approximates a baseband white random process when the pilots and guard interval are excluded. This type of signal approximates a thumbtack form of the Ambiguity Function (AF), and it exhibits promising radar waveform properties. The introduction of the deterministic components such as pilot tones and guard interval, produces ambiguities outside zero range and Doppler. A target response will therefore produce several ambiguities outside the position of the target, but these are deterministic in range and Doppler and it has been shown how to cope with them [12], [26, pp 315-317].

## III. PASSIVE BISTATIC RADAR

Range walk is a phenomenon occurring when the range resolution is fine compared to the velocity of the target

and the integration time. Range walk leads to an energy dispersal in the range correlation, and bistatic range walk occurs when the following inequality is fulfilled,

$$\frac{c}{B} < v_B T_I \tag{1}$$

where $c$ is the speed of propagation, $B$ is the bandwidth, $v_B$ is the bistatic velocity of the target, and $T_I$ is the coherent integration time. From (1), a high velocity target can be defined as a target moving through several range bins during integration.

Bistatic Doppler walk occurs when the target accelerates through several Doppler bins during integration, and this also leads to an energy dispersal in both the range (minor) and velocity (major) correlation. Doppler walk occurs when

$$\frac{\lambda}{2} < T_I^2 a_B \tag{2}$$

where $\lambda$ is the wavelength of the signal, $T_I$ is the coherent integration time and $a_B$ is the target's bistatic acceleration. From (2), a highly accelerated target can be defined as a target moving through several Doppler bins during integration.

## IV. SIMULATED DATA ANALYSIS

In this analysis, a software DVB-T signal generator was implemented in Matlab according to [27]. Random bits were used as the data stream, which is a good approximation according to [26, pp 322]. The radar signal processing algorithm presented in [28] was used both for simulated and real data analysis. The reference signal was a copy of the simulated DVB-T signal and Additive White Gaussian Noise (AWGN). The surveillance signal consisted of two parts. The first was a copy of the simulated DVB-T signal, to simulate the Direct Signal Interference (DSI). The second part was a time dependent time and frequency shift to simulate the target's movement during the integration time. The adjustable parameters is carrier frequency, target echo amplitude, noise amplitude, bistatic range, bistatic velocity and bistatic acceleration.

Figure 1 shows the $(S/N)_{\max}$ of the target versus coherent integration time, where $(S/N)_{\max}$ is defined as the maximum integrated signal to noise ratio of the target. A doubling of the coherent integration time optimally results in a $3dB$ gain [29] for a stationary targets, which in figure 1 is shown as the reference curve. The dashed line shows the $(S/N)_{\max}$ of the target, and the solid line shows the reference. The target $(S/N)_{\max}$ follows the reference up to 0.5 seconds of integration time, but after that $(S/N)_{\max}$ falls off as the integration time increases, and this is due to the range walk.

Figure 2 shows the target $(S/N)_{\max}$ versus integration time. The dashed line is the target, and the solid line is the reference. The target $(S/N)_{\max}$ follows the reference up to 0.2 seconds of integration time, but after that $(S/N)_{\max}$ falls off as the integration time increases, and
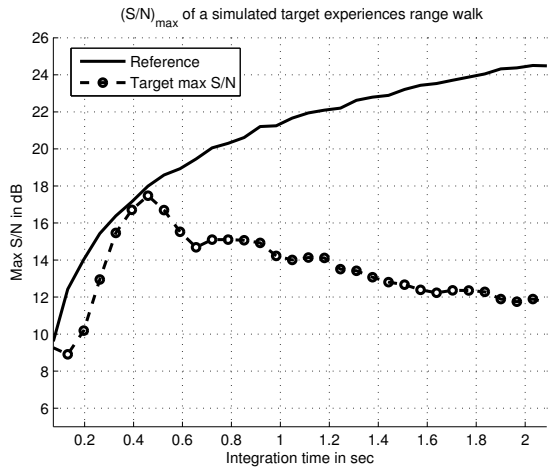
Fig. 1. $(S/N)_{\max}$ versus integration time of a simulated target, illustrating range walk. $v_B \approx 100 m/s$
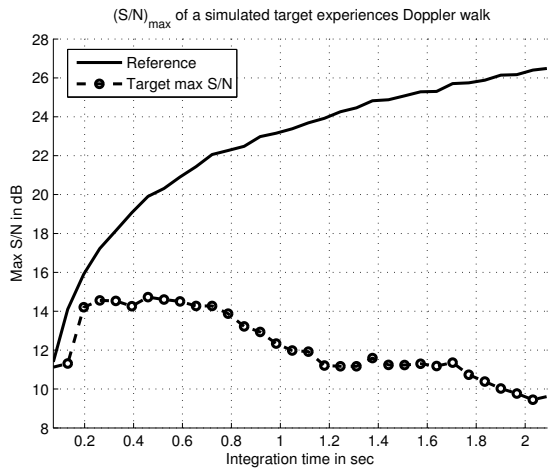


Fig. 2. $(S/N)_{\max}$ versus integration time of a simulated target, illustrating Doppler walk. $a_B \approx 6 m/s^2$
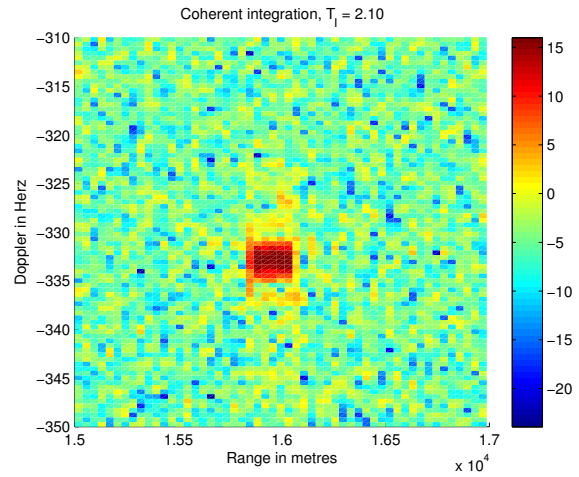


Fig. 3. Coherent integration over an interval $T_I = 2.1s$, of a simulated target. Amplitude in $dB$.
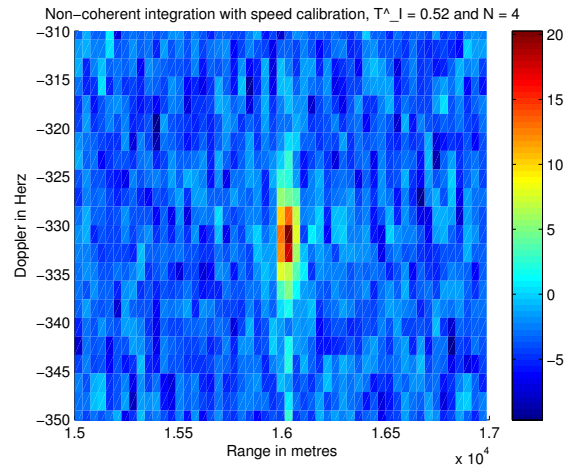


Fig. 4. Non-coherent integration with speed calibration, $\hat{T}_I = 2.1/4s = 0.52s$, of a simulated target. Amplitude in $dB$.

this caused by the Doppler walk.

The effect of range walk is seen as loss of $(S/N)$ in the correlation when the coherent integration time is increased. The velocity of each cell in the correlation is known, and this information can be used to maximize the $(S/N)$ when range walk causes energy dispersal in the correlation, and this method is in the following referred to as non-coherent integration with speed calibration.

Instead of coherently integrate over the time $T_I$, the method divides the integration interval in $N$ segments where each segment has an integration time of $\hat{T}_I = \frac{T_I}{N}$. Each segment is then coherently integrated, and subsequently a method for compensating and non-coherently integrating these intervals is applied. Defining $\hat{\chi}(m, n)_k$ as the coherent integration of the $k$'th coherent integration interval with integration time of $\hat{T}_I$. The speed calibrated

correlation can be written

$$\hat{\chi}(m,n)_{SC} = \sum_{k=0}^{N-1} \left| \hat{\chi}(m, n - \lfloor \frac{B}{f_c} mk \rfloor)_k \right| \qquad (3)$$

where $B$ is the signal bandwidth, $f_c$ is the signal carrier frequency and $\lfloor x \rfloor$ is the floor of $x$. The operation of non-coherent integration yields a theoretical gain of $1.5dB$ for each doubling of the integration time. This method assumes no Doppler walk during each segment integration time.

Figure 3 shows an integration of a simulated high velocity target (see (1) for definition of high and low velocity target) over an integration interval of 2.1 seconds. Clearly, the target is spread over several range bins because of the range walk.

Figure 4 shows an integration using non-coherent integration with speed calibration applied on the same dataset as in figure 3. Comparing figures 3 and 4 shows that
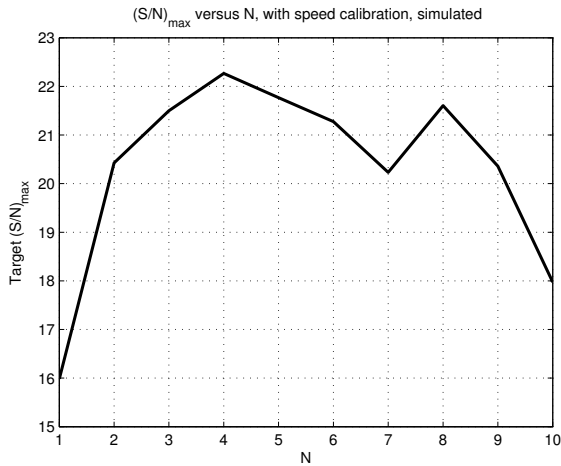
Fig. 5. Non-coherent integration with speed calibration, $(S/N)_{max}$ versus $N$ for $T_I = 2.1s$, of a simulated target.



Fig. 6. Coherent integration of a high velocity target, with $T_I = 2.10s$, illustrating range walk. Amplitude in $dB$.

using the method of non-coherent integration and speed calibration on a high bistatic velocity target, the energy is more focused and the $(S/N)_{max}$ is increased.

Figure 1 shows that the optimum coherent integration time is approximately $0.5s$ for this target's bistatic velocity. This information can be used to calculate the optimum choice of $N$, given the wanted $T_I$. For a required integration interval $T_I$ and a given optimum coherent integration time $\hat{T}_I$, $N$ is subsequently calculated by

$$N = \lfloor \frac{T_I}{\hat{T}_I} \rfloor \qquad (4)$$

Where $\lfloor x \rfloor$ is the floor operator. In case of required integration time $T_I = 2.1s$, for our target, where $\hat{T}_I = 0.5s$, the optimum $N = 4$. Figure 5 shows target $(S/N)_{max}$ versus $N$, for $T_I = 2.1s$, and we can clearly see from the figure that the optimum choice for $N$ is 4 as calculated. The secondary peak at $N = 8$ is for the moment of unknown origin, but probably due to the waveform which is based on $2^M$, where $M$ is an integer, samples for this sampling frequency. The figure is produced for a single case, and not statistically.

The maximum gain attainable for this method versus coherent integration is $log_2(N) \times 1.5dB$, subtracted the difference in $(S/N)_{max}$ for integrating coherently over $T_I$ versus integrating coherently over $\hat{T}_I$. This is given as

$$G_{SC}(T_I, N) = log_2(N) \times 1.5dB - \Delta(S/N)_{max}(T_I, N) \quad (5)$$

where $T_I$ is the coherent integration time, $N$ is the number of segments to split $T_I$ into and $\Delta(S/N)_{max}(T_I, N)$ is given as

$$\Delta(S/N)_{max}(T_I, N) = (S/N)_{max}(T_I) - (S/N)_{max}(\frac{T_I}{N}) \quad (6)$$

where $(S/N)_{max}(T)$ is the target maximum $S/N$ for coherent integration time of $T$.

From figure 1, we see that the difference in $(S/N)_{max}$ for $T_I = 2.1s$ and $\hat{T}_I = 0.52s$ is approximately $-4dB$. The
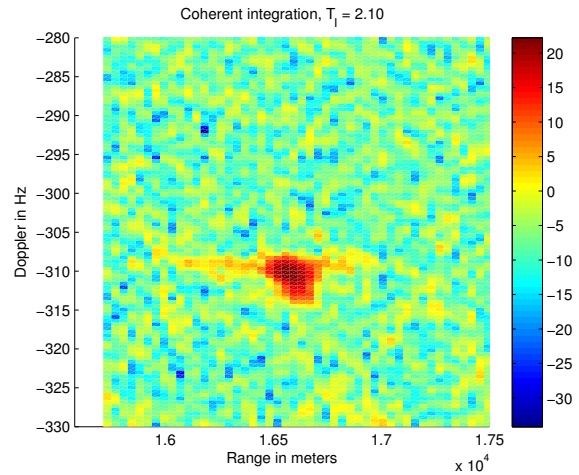
maximum gain attainable for this method versus coherent integration over $T_I$ is $log_2(4) \times 1.5dB + 4dB = 7dB$. Figure 5 shows a difference in gain from $N = 4$ (speed calibrated) and $N = 1$ (coherent integration) of approximately $6.2dB$. This is close to the theoretical gain attainable of $7dB$.

## V. Experimental data analysis

Real life data was collected using an experimental data recording system described in greater detail in [30], [31]. Two geometries were used with baselines of approximately $20km$ and $50km$. Standard TV antennas were used, and terrain shielding were used to reduce the DSI. The receiver site was close to a small airplane airport, with commercial airliner traffic passing on their way to a larger airport, and all target's reported here are target's of opportunity passing the surveillance antenna.

Figure 6 shows a high velocity target (see (1) for definition) with coherent integration time of $2.1s$, and we see that the target moves through several range bins during integration. Figure 7 shows the same target at the same time with a shorter coherent integration time. We see that the plot with longer integration time has larger range dispersion than shorter coherent integration time.

Figure 8 shows the target $(S/N)_{max}$ versus coherent integration time, and the gain flattens compared to the reference value after $T_I \approx 0.5s$.

Figure 9 shows a highly accelerated target (see (2) for definition) with coherent integration time of $2.1s$, and we see that the target moves through several Doppler bins during integration. Figure 10 shows the same target at the same time with coherent integration time $0.26s$. We see that the plot with longer coherent integration time has a larger Doppler spread than the shorter coherent integration time.
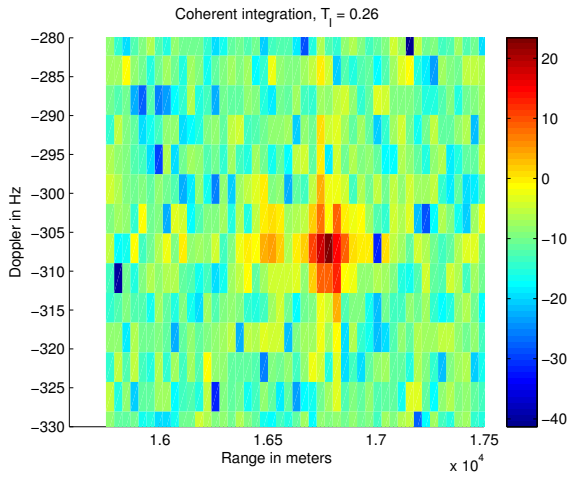
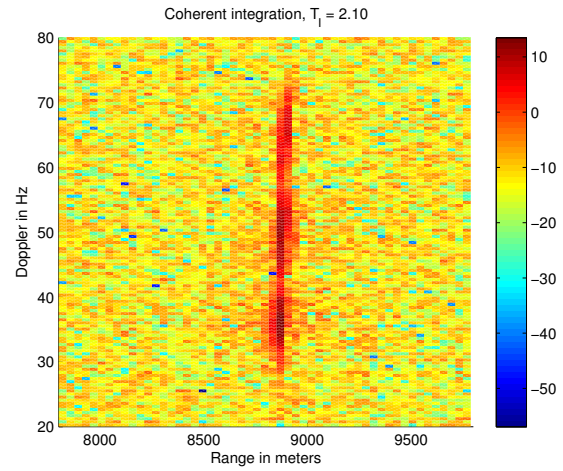Fig. 7. Coherent integration of a high velocity target, with $T_I = 0.26s$, illustrating range walk. Amplitude in $dB$.



Fig. 9. Coherent integration of a highly accelerated target, with $T_I = 2.10s$, illustrating Doppler walk. Amplitude in $dB$.
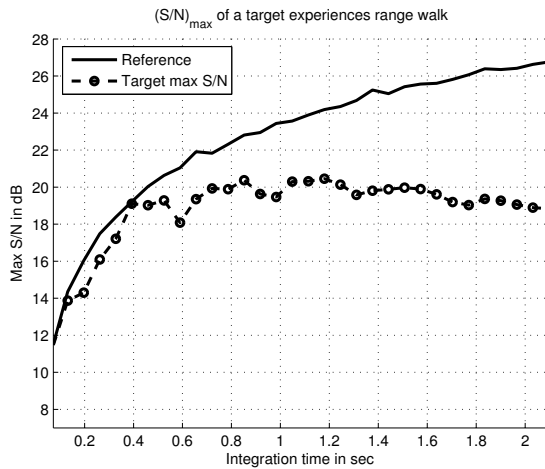


Fig. 8. $(S/N)_{max}$ versus integration time of a target, illustrating range walk. $v_B \approx 100m/s$



Fig. 10. Coherent integration of a highly accelerated target, with $T_I = 0.26s$, illustrating Doppler walk. Amplitude in $dB$.

Figure 11 shows the target $(S/N)_{max}$ versus integration time, and the gain falls of from the reference value after $T_I \approx 0.3s$.

Next, we apply the method of non-coherent integration with speed calibration on the range walk dataset from figure 8. Non-coherent integration with speed calibration assumes that no Doppler walk occurs, and for long integration times, this is not realistic. When integration time $T_I$ is large, and the integration time of each segment, $\hat{T}_I$, is smaller, it is probable that the target energy is in different Doppler cells for each coherent integration interval, which is a violation of the assumption of the method of non-coherent integration with speed calibration. The solution is to perform a filter in Doppler of each $\hat{\chi}(m,n)_k$, such that the target smears in Doppler. The filter can be a moving average filter of the type described in the following equation.
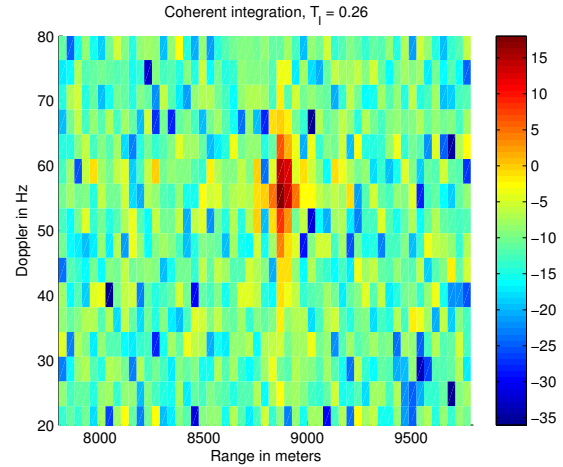
$$|\tilde{\chi}(m,n)_k| = \frac{1}{M} \sum_{l=0}^{M-1} |\hat{\chi}(m-l,n)_k|, \quad \text{for all} \quad m,n \quad (7)$$

where $\tilde{\chi}(m,n)_k$ is the Doppler filtered version of $\hat{\chi}(m,n)_k$ and $M$ is the size of the moving average filter. The target is spread over $M$ Doppler bins in order to ensure target response in range for a span of Doppler velocities.

Figure 6 shows coherent integration with integration time of $T_I = 2.1s$ for a target. The target moves through several range bins during integration, and the effects of range walk is clear from figure 8, where we see that the $(S/N)_{max}$ for $T_I = 2.1s$ is approximately $7dB$ lower than the reference. Using the method of non-coherent integration with speed calibration focuses the energy for each correlation, and the resulting correlation is given in figure 12, where $T_I = 2.1s$ and $N = 5$. The target range response in figure 8 is over several range bins, and
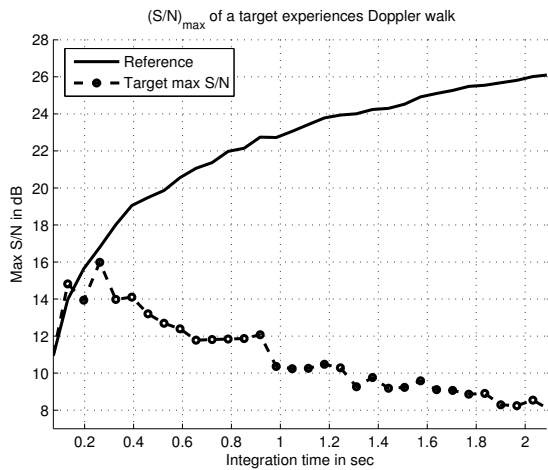
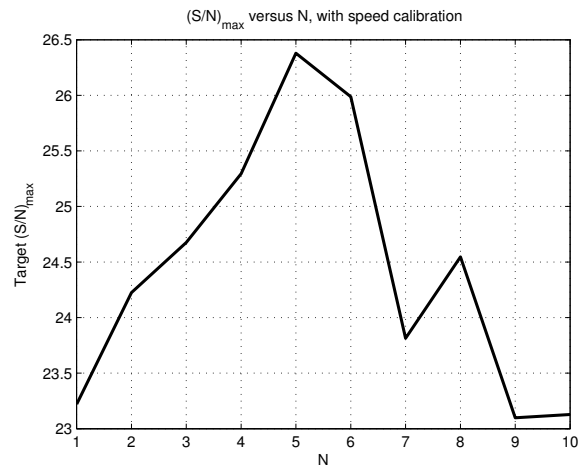Fig. 11. $(S/N)_{\max}$ versus integration time of a target, illustrating Doppler walk. $a_B \approx 6m/s^2$



Fig. 13. Non-coherent integration with speed calibration, $(S/N)_{\max}$ versus $N$ for $T_I = 2.1s$, of a target.
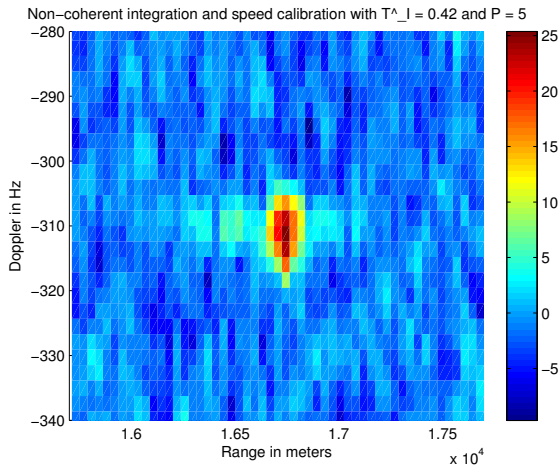


Fig. 12. Non-coherent integration with speed calibration, $\hat{T}_I = 2.1/5s = 0.42s$ of a target. Amplitude in $dB$.

compared to the range response in figure 12 where non-coherent integration with speed calibration is applied, the energy is clearly more focused in range.

Figure 13 shows $(S/N)_{\max}$ versus $N$ for a high velocity target, used in the range walk analysis. $N = 1$ is the standard coherent integration over the entire interval $T_I$, and $N = 5$ is the case given in figure 12. The figure shows that the optimum choice for $N$ in this case is 5, and this can also be read from figure 8 where the target $(S/N)_{\max}$ falls off after reaching $T_I/N = 2.1/5 = 0.42s$ seconds. As already noted in the simulated data analysis chapter, a possible reason for the occurrence of the secondary peak at $N = 8$ is the waveform properties of the DVB-T signal, where the symbol length is of the form of $2^M$, where $M$ is an integer, samples for this sampling frequency. The figure shows the result from one single target, and it is not the result of a statistical study.

The $(S/N)_{\max}$ gain from coherent integration over $T_I$

to non-coherent integration is approximately $3.3dB$. From figure 8, the difference in $(S/N)_{\max}$ from integration time of $T_I = 2.1s$ versus $\hat{T}_I = \frac{T_I}{N} = 2.1s/5$ is approximately $0dB$. Equations for calculating the theoretical gain from using the method of non-coherent integration with speed calibration versus coherent integration over $T_I$ is given in (5) and (6). From figure 13, the gain achieved using this method is approximately $3.2dB$, which is close to the theoretically attainable gain of $log_2(5) \times 1.5dB - 0dB \approx 3.48dB$.

## VI. CONCLUSION

A PBR system based on the DVB-T system will face problems with range and Doppler walk due to the relatively long integration time (up to and maybe longer than $1s$), which will lead to high Doppler resolution. The long integration time also results in the target moving through several range resolution cells due to the relatively high bandwidth of the DVB-T system. The effects of range and Doppler walk is energy dispersal in the correlation and loss of target $(S/N)_{\max}$, and is presented in sections 4 and 5 for both simulated and experimental data. The lower signal to noise ratio is a problem, because probability of detection is dependent on the signal to noise ratio.

This work described a method of non-coherent integration with speed calibration which showed an improvement on the $(S/N)_{\max}$ for long integration times and high velocity targets in comparison to coherent integration over the integration interval. The improvement on $(S/N)_{\max}$ were close to the theoretical gain of non-coherent integration for stationary targets, even for longer processing times and high velocity targets.

## REFERENCES

[1] N. Willis and H. D. Griffiths, editors. *Advances in Bistatic Radar*. Scitech Pub Inc, 2007.
[2] N. J. Willis. *Bistatic Radar*. Technology Service Corporation, Silver Spring, MD, USA, 1995.

[3] Nicholas J. Willis and Hugh D. Griffiths. *Advances in Bistatic Radar*. 2007.

[4] Nicholas J. Willis. *Bistatic Radar, 2nd Edition*. 1995.

[5] Silent Sentry. Innovative Technology for Passive, Persistant Surveillance, June 2005.

[6] J.M. Ferrier, M. Klein, and S. Allam. Frequency and Waveform Complementarities for Passive Radar Applications. pages 1–6, September 2009.

[7] H. D. Griffiths. From a different perspective: Principles, practice and potential of bistatic radar. In *Proc. International Radar Conference*, September 2003.

[8] C. J. Baker and H. D. Griffiths. Bistatic and Multistatic Radar Sensors for Homeland Security. July 2005.

[9] H. D. Griffiths and C. J. Baker. Passive coherent location radar systems. Part 1: Performance prediction. *IEE Proc.-Radar Sonar Navig.*, 152(3):153–159, June 2005.

[10] C. J. Baker and H. D. Griffiths and I. Papoutsis. Passive coherent location radar systems. Part 2: Waveform properties. *IEE Proc.-Radar Sonar Navig.*, 152(3):160–168, June 2005.

[11] H. D. Griffiths and C. J. Baker. The Signal and Interference Environment in Passive Bistatic Radar. pages 1–10, February 2007.

[12] R. Saini and M. Cherniakov. DTV signal ambiguity function analysis for radar application. *IEE Proc.-Radar Sonar Navig.*, 152(3):133–142, June 2005.

[13] A. Lauri and F. Colone and R. Cardinali and C. Bongioanni and P. Lombardo. Analysis and Emulation of FM Radio Signals for Passive Radar. pages 1–10, March 2007.

[14] T. Tsao and M. Slamani and P. Varshney and D. Weiner and H. Schwarzlander and S. Borek. Ambiguity function for a bistatic radar. *IEE Trans. Aerospace and Electronic Systems*, 22(3):1041–1051, July 1997.

[15] F. Colone, D. W. O'Hagan, P. Lombardo, and C. J. Baker. A multistage Processing Algorithm for Disturbance Removal and Target Detection in Passive Bistatic Radar. *Aerospace and Electronic Systems, IEEE Transactions on*, 45(2):698–722, April 2009.

[16] D.W. O'Hagan, F. Colone, C. J. Baker, and H.D. Griffiths. Passive Bistatic Radar (PBR) demonstrator. pages 1–5, October 2007.

[17] D. W. O'Hagan and C. J. Baker. Passive Bistatic Radar (PBR) using FM radio illuminators of opportunity. pages 1–6, October 2008.

[18] C. Bongioanni and F. Colone and P. Lombardo. Performance Analysis of a Multi-Frequency FM Based Passive Bistatic Radar. pages 1–6, May 2008.

[19] P. Lombardo and F. Colone and C. Bongioanni and A. Lauri and T. Bucciarelli. PBR activity at INFOCOM: adaptive processing techniques and experimental results. pages 1–6, May 2008.

[20] D. Gould and R. Pollard and C. Sarno and P. Titte. Developments to a Multiband Passive Radar Demonstrator System. pages 1–5, October 2007.

[21] M. Edrich and F. Wolschendorf and A. Schröder. FM and DAB Experimental Passive Radar System: Concept and Measurement Results. pages 1–4, September 2009.

[22] M. Cherniakov, editor. *Bistatic Radar: Emerging Technology*. John Wiley & Sons Ltd, 2008.

[23] M. Cherniakov, editor. *Bistatic Radar: Principles and Practice*. John Wiley & Sons Ltd, 2007.

[24] D. R. Wehner. *High-Resolution Radar*. Artech House, Norwood, MA, USA, 2 edition, 1995.

[25] Urkowitz H. Noncoherent Correction of Radar Range Walk Using Digital Processing. volume 18, pages 470–474.

[26] Mikhail Cherniakov. *Bistatic Radars: Emerging Technology*. 2008.

[27] ETSI. Digital video broadcasting (dvb); framing structure, channel coding and modulation for digital terrestrial television. 300 744 v1.5.1, 2004-11.

[28] K. E. Olsen, T. Johnsen, S. Johnsrud. Details of the signal processing, simulations and results from the Norwegian multistatic radar DiMuRa. *Proceedings of the IEEE Waveform Diversity and Design Conference*, February 2006.

[29] Nadav Levanon. *Radar Principles*. 1988.

[30] K. E. Olsen, C. J. Baker. FM-based Passive Bistatic Radar as a function of available bandwidth. *Proc. of IEEE Radar Conference*, May 2008.

[31] K. E. Olsen, K. Woodbridge. FM Based Passive Bistatic Radar Target Range Improvement. *Proc. International Radar Symposium*, September 2009.